Article

Polarized light and X-ray precession study of the ferroelastic domains of YBa2Cu3O7-?

SCHMID, Hans, *et al*.

Abstract

The ferroelastic domains of the orthorhombic phase of YBa2Cu3O7-δ were obsd. in polarized light on ceramics and single crystals. By combining polarized light microscopy with the x-ray presession technique, the correlation of the orientation of the orthorhombic a- and b-axes with that of the a-b-plane bireflectance, reflection dichroism, transmission dichroism, reflection tints generated with compensators and on uncrossing of polars, as well as the orientation of etch pits was realized on ferroelastic single domains, bi-domains, and more complicated domain patterns. Four ferroelastic orthorhombic domain states were identified, at variance with former group theor. considerations, predicting only 2 states. Ensembles of lamellar domains beyond optical resoln. generate strong bireflectance with principal axes rotated by 45° relative to the true a,b-directions.

Reference

UNIVERSITÉ DE GENÈVE

Polarized light and X-ray precession study of the ferroelastic domains of $YBa_2Cu_3O_{7-\delta}$

H. Schmid[1], E. Burkhardt[1], E. Walker[2], W. Brixel[1], M. Clin[1], J.-P. Rivera[1], J.-L. Jorda[2], M. François[3], and K. Yvon[3]

[1] Université de Genève, Département de Chimie Minérale,
Analytique et Appliquée, Genève, Switzerland

[2] Université de Genève, Département de Physique de la Matière Condensée,
Genève, Switzerland

[3] Université de Genève, Laboratoire de Cristallographie aux Rayons-X,
Genève, Switzerland

Received December 22, 1987

The ferroelastic domains of the orthorhombic phase of $YBa_2Cu_3O_{7-\delta}$ have been observed in polarized light on ceramics and single crystals. By combining polarized light microscopy with the X-ray precession technique, the correlation of the orientation of the orthorhombic a- and b-axes with that of the $a-b$-plane bireflectance, reflection dichroism, transmission dichroism (at a thickness of about 1 μm), reflection tints generated with compensators and upon uncrossing of polars, as well as the orientation of etch pits has been realized on ferroelastic single domains, bi-domains and more complicated domain patterns. Four ferroelastic orthorhombic domain states have been identified, at variance with former group theoretical considerations, predicting only two states. Ensembles of lamellar domains beyond optical resolution generate strong bireflectance with principal axes rotated by 45° relative to the true a, b-directions.

1. Introduction

Following the discovery of the high T_c superconductive properties of $YBa_2Cu_3O_{7-\delta}$ (YBCO), numerous workers [1-4, 29, 30] found by means of electron microscopy that its orthorhombic phase was composed of extremely thin twin lamellae with a width down to about 20 nm and (110) composition planes (domain walls). The formation of domains is a normal phenomenon occurring during non-destructive ferroic phase transitions involving symmetry reduction, i.e. usually upon cooling. In such a case the "twinning laws" of the ferroic phase – i.e. the symmetry operations to transform one domain into all others – are given by the symmetry elements lost during the transition. However, the tetragonal→orthorhombic phase transition of $YBa_2Cu_3O_{7-\delta}$, occurring at about 700 °C at ~1 bar of oxygen [5], has to some extent a destructive character because it is linked with a

chemical reaction involving oxygen loss$\rightleftharpoons$absorption:

$$YBa_2Cu_3O_7 \rightleftharpoons YBa_2Cu_3O_{7-\delta} + \delta/2\ O_2.$$
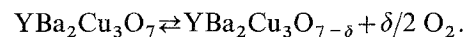
Thus it is not evident at first sight whether the symmetry argument holds, but considering the topotactically reversible behaviour of this reaction, the skeleton of the tetragonal basic structure remaining fully preserved [6], the point group relationship $4/mmm \leftrightarrow mmm$ of the two chemically non-identical phases can safely be taken as the determinative species for the twinning laws. The change of crystal system at the phase transition necessarily requires the ferroic phase to be of ferroelastic character. The equi-translation nature of the transition [6] means that no anti-phase-domains, generated by the phase transition, would be allowed [7].

According to Aizu [8] the number of ferroic domain states is obtained by the ratio of the point group

orders of the high symmetry and low symmetry phases. On this basis one expects two ferroelastic domain states for orthorhombic $YBa_2Cu_3O_7$.

Following Fousek and Janovec [9, 10] who determined the mechanically allowed walls of ferroelectric ferroelastics, Sapriel [11] generalized the analysis and determined the number and orientation of the mechanically allowed domain walls of all 94 Aizu species of full ferroelastics. For the species $4/mmmFmmm$ of YBCO one finds in Sapriel's tables that only two walls, i.e. parallel (110) and ($1\bar{1}0$) are allowed for linking the two expected [8] domains. Indeed, most of the electron microscopy work and our own polarized light studies confirm the presence of only these two equivalent kinds of wall. Surprisingly, however, four domain states instead of the expected [8] two ones, have been observed by X-ray precession photographs [12, 31, 32]. According to Aizu [8] the formation of four domains would be possible in tetragonal $\rightarrow$ monoclinic transitions and lead to either 8 or 9 walls [11]. From symmetry considerations by Gratias and Portier [11a] on martensitic transformations, which can be assimilated to ferroelastic phase transformations, it becomes clear that the number of orientational twins is not universally determined by the ratio of point group orders (i.e. by the index) of the prototypic and ferroic phases. Recently, Shuvalov et al. [13] came to similar conclusions and demonstrated with examples that real ferroelastic crystals in fact often develop a higher number of domain states (concept of "superorientational states") than hitherto [8, 11] believed. Therefore, it is important to consider whether orthorhombicity is sufficient to explain the twinning of YBCO or whether the structure has in reality a symmetry lower than orthorhombic.

From electron microscopy work, the occurrence of (001) walls, linking orthorhombic domains with interchanged a- and b-axes, has been inferred [14, 14a] and evoked in connection with the "glassy state" problem [15]. Such walls are not mechanically allowed for species $4/mmmFmmm$. If they really do occur, this would mean strong mechanical frustration and be expected to lead to a strongly strained or a stress-induced tetragonal transition zone. Allowed (001)-walls are only permitted for tetragonal $\rightarrow$ monoclinic point group combinations such as $4/mmmF2/m(s)$, where the monoclinic b-axis is perpendicular to tetragonal [001].

In the present paper different possibilities of optical contrast formation – based on bireflectance and dichroism in reflection and transmission – between the ferroelastic domains of YBCO have been studied and correlated with the orientation of the crystallographic axes. By combining these optical findings with the X-ray precession technique, different types of domain pattern will be analysed and shown to be explicable without the needing to assume a symmetry lower than orthorhombic.

2. Sample preparation

2.1. Ceramics

With a view to revealing the ferroelastic domain structure in polarized light, two ceramic samples were studied initially. Their preparation was as follows:

Sample A: A stoichiometric mixture of CuO($>99\%$), Y_2O_3 (5 N) and $BaCO_3$($>99\%$) – all from Fluka –


Plate I/1a–c. Ceramic YBCO sample A, in reflected light (Xe-lamp), **a** without analyser, note inclusions in large crystallite, **b** crossed polars, large crystallite in "diagonal" orientation, polars $\parallel$ [110], (compare part 7.8!) **c** large crystallite nearly in extinction, polars $\parallel$ [100], "puzzle" domains in upper left hand area

Plate I/2. Ceramic YBCO (sample B) in tetragonal state, reflected light (Xe-lamp), crossed polars, some crystallites in extinction position (dark), absence of domain walls

Plate I/3a–e. Crystal 4, "puzzle" domains only, **a** polarizer $\parallel$ [110] alone, weak reflexion dichroism of pseudo-symmetry visible: bluish and pinkish areas, identical to dark and clear areas of 3c, respectively, for vibration direction of polarizer indicated, **b** crossed polars $\parallel$ [110]/[$1\bar{1}0$], **c** analyser anticlockwise uncrossed from crossed polars orientation $\parallel$ [100]/[010], **d** polars crossed $\parallel$ [100]/[010], **e** analyser clockwise uncrossed

Plate I/4a–e. Crystal 5. Combination of large single domain areas with square of "puzzle" domain areas. **a** crossed polars $\parallel$ [110]/[$1\bar{1}0$], no compensator **b** and **c** idem **a** but with Berek compensator inserted; γ-direction of Berek indicated **d** clockwise and **e** anticlockwise uncrossed polars, starting from position with crossed polars $\parallel$ [100]/[010]. Errata in 4a: the analyser/polarizer orientation of I/4a is identical to that of I/4b and I/4c

Plate I/5a–c. YBCO (001) facet with partly transparent decomposition layer; walls indicate 110-directions; **a** unpolarized light, **b** polars crossed $\parallel$ [110]/[$1\bar{1}0$], **c** idem **b** but de Sénarmont compensator inserted: contrast between domains still possible (top: grey, bottom: coloured)
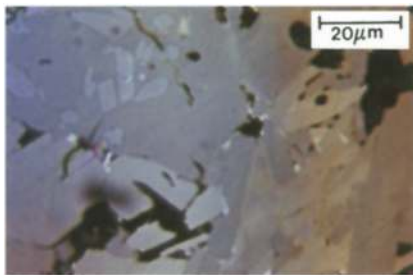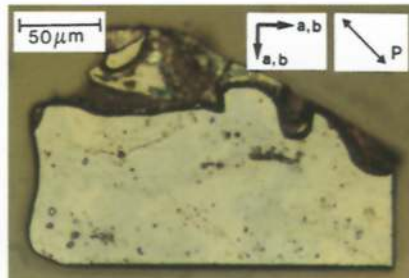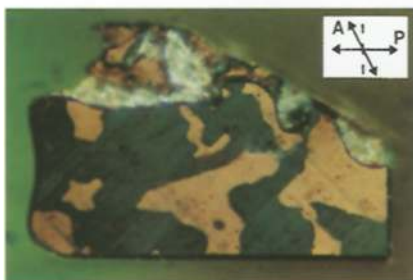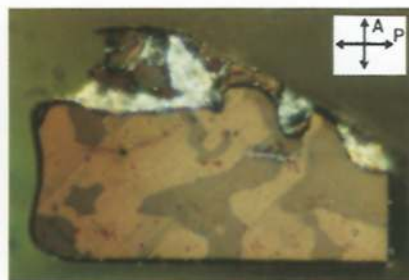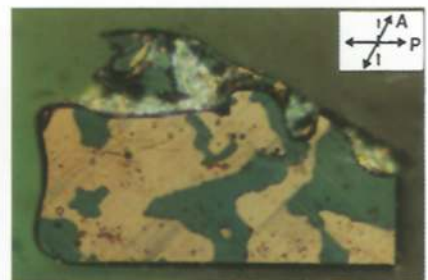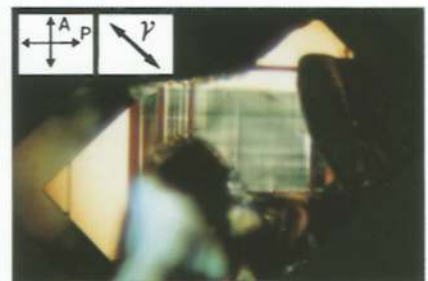
1a

1b

1c
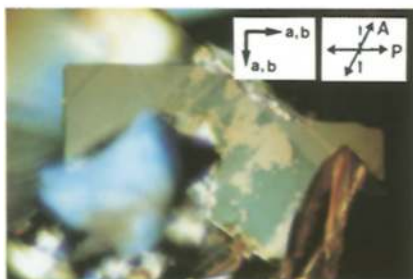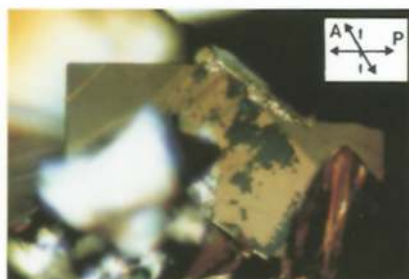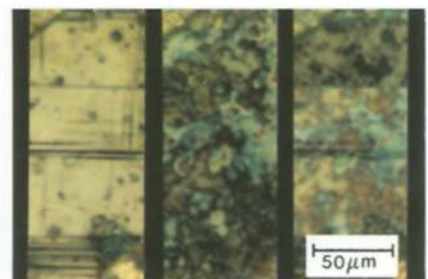
2

3a

3b

3c

3d

3e
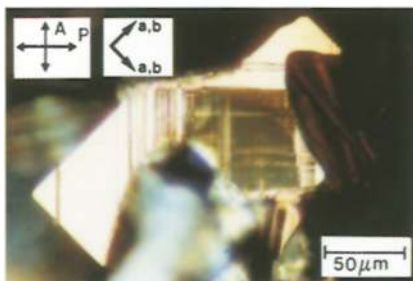
4a

4b

4c

4d

4e

5a   5b   5c

was fired for 20 h at 950 °C in air, crushed, pressed and refired for 16 h at 950 °C in O_2-flow, followed by a 1 h anneal at 1020 °C in O_2 and cooling at 50 °C/h to room temperature.

Sample B: Same mixture and prefiring as for sample A, but rapid cooling (200 °C/min) in air.

For study under the microscope the samples were embedded in plexi-glass, ground, and polished with diamond paste.

2.2. Single crystals

Several ways of growing single crystals of YBCO have been described [16, 17, 18, 19], all of which use melts with an excess of CuO. In the present study the procedure described by Damento et al. [16] was followed. Two slightly different experiments were run:

Experiment I. 20 g of a mixture of 42% $BaCO_3$, 46% CuO and 12% Y_2O_3 were heated in a 10 ml platinum crucible for 1 h at 1150 °C, followed by quenching in air. After remarking that only a small fraction of the initial charge had melted and with a view to increasing the melted part, the crucible was reheated in a high frequency furnace without temperature control, but observing continuously the state of the charge. Upon increasing monotonically the RF power, a sudden temperature increase was observed, probably due to the onset of RF-coupling to the more and more conducting melt. The RF power was immediately reduced in order to protect the platinum crucible, but during the temperature excursion the liquefied part of the charge had increased. This process was repeated until almost all of the material appeared to be liquid. Thereafter the crucible was held at 900 °C for four days, followed by cooling at 1 °C/min to room temperature in air.

Experiment II. About 30 g of the thoroughly ground mixture (see above) were melted at 1150 °C in a flat platinum boat, air quenched and subsequently annealed at 900 °C during 4 days. The annealing period was followed by cooling at 1 °C/min to room temperature.

In both experiments the free upper surface of the charge was covered with many needle-like monoclinic CuO-crystals (1–2 mm long, ~0,1 mm thick), attached to which a smaller number of square and rectangular plates of YBCO crystals (edge length up to 100 µm, thickness ~1–3 µm) with very flat and shiny surfaces had grown in an essentially unhindered way, probably by some kind of surface film diffusion process. Inside the solidified cakes smaller and less perfect crystals with growth steps, ressembling those reported by other workers [16, 17], had formed. The crystals used for the optical studies were removed from the copper oxide by careful brushing of the surface. Measurements of T_c of the studied crystals were not made individually but other crystals of the same batches were dispersed in liquid nitrogen, contained in a glass test tube. The plate-like crystals stuck to the walls and could be moved by means of a ferrite magnet from outside the tube. Thus T_c was certainly well above 77 K.

3. Polarized light studies of ferroelastic domains in reflected light

3.1. Ceramics

Our initial studies of the domain structure of YBCO have been made on ceramics. Two representative samples (see 2.1) will be described.

Sample A (Plate I/1a–c). By observing with crossed polars, the randomly oriented crystals extinguish at

---

Plate II/6a–c. Single crystal with rectangular etch pits inside single domains, crossed polars, in diagonal position; mounted with silicon rubber on a glass capillary, **a** front side and **b** back side, **c** back side with de Sénarmont compensator inserted; heavily twinned triangular area (left hand) stays always dark. Note that the (110)-walls go right through the entire thickness of the crystal

Plate II/7a–c. Crystal 2. Stress and strain free arrangement of domains with one kind of (110) walls. Vivid blue-yellow contrast with Laves-Ernst compensator (see Table 2). With X-rays→double spots (Fig. 3)

Plate II/8a–h. "Puzzle domain" crystal, idem Plate I/3a–e, but with Laves-Ernst compensator (a–f) and de Sénarmont compensator (g, h), **a** and **b** n_y of compensator $\|a, b$ with addition and subtraction position, resp.; **c** and **d**: idem **a**, **b** but crystal slightly rotated on stage: **e** and **f**, n_y of compensator $E - W$, interchange of colours (e)↔(f) after 90°-rotation of crystal on stage; **g** and **h**: idem e/f but with de Sénarmont compensator
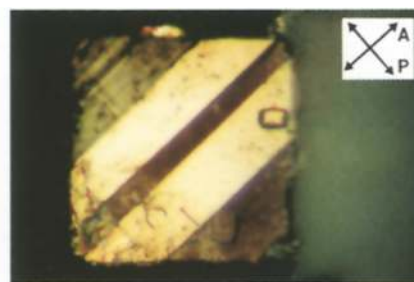
Plate II/9a–c. Contrast between single domains by means of the de Sénarmont compensator **a** addition for large domain, **b** no compensator, **c** subtraction for large domain; high density of walls in left hand bottom triangle. Errata: in 9a and 9c the analyser is infact uncrossed, starting from position 9b
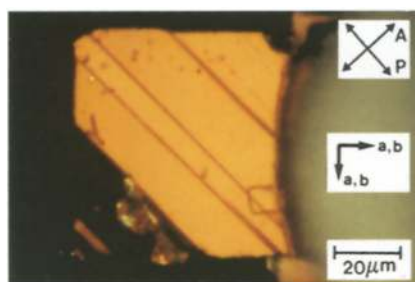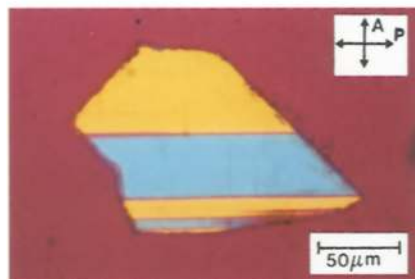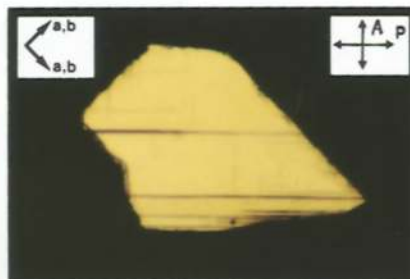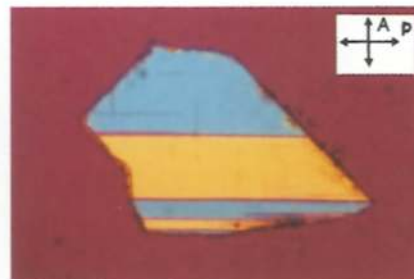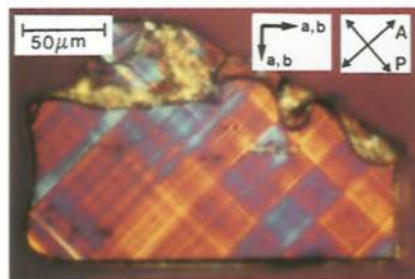
6a
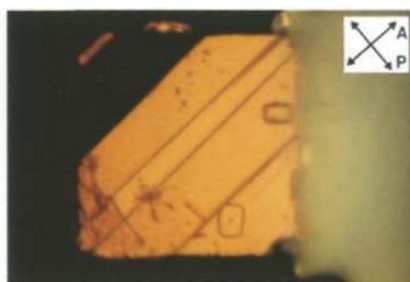
6b

6c

7a

7b

7c

8a
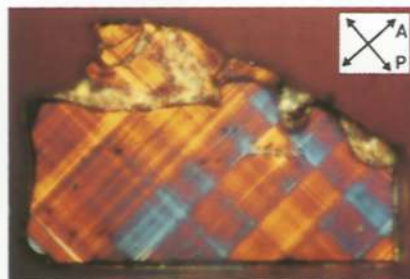
8b
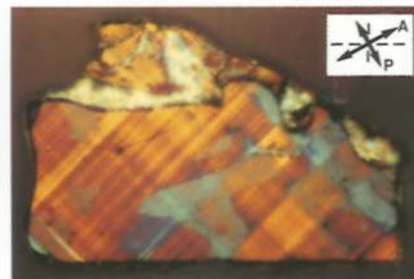
8c
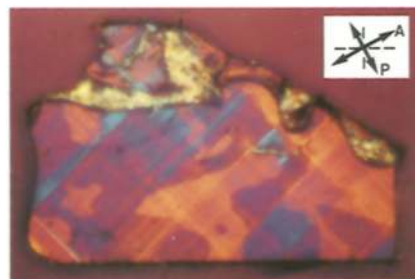
8d
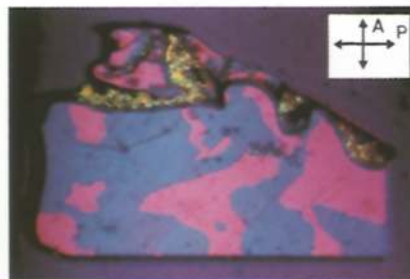
8e
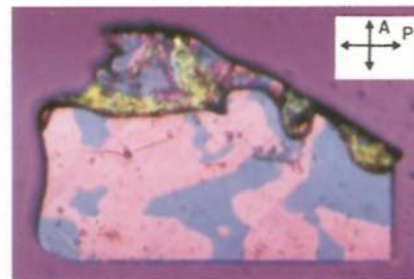
8f
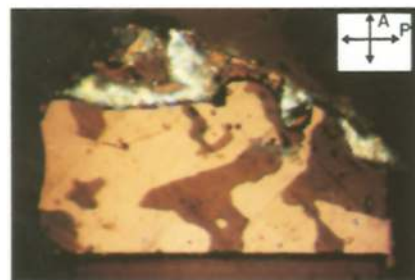
8g
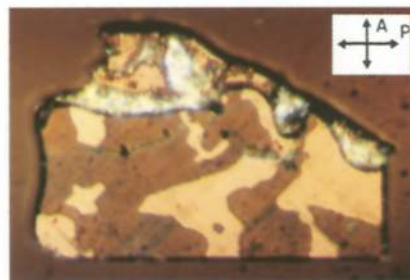
8h
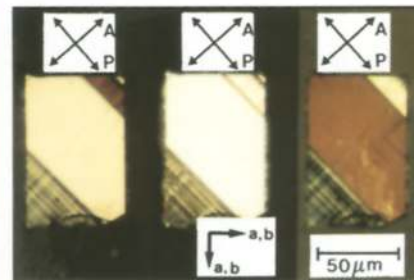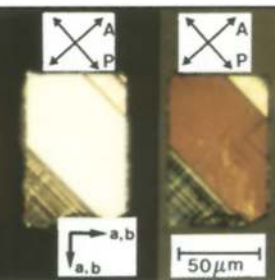
9a   9b   9c

different positions of the microscope stage. In non-extinction positions, particularly in the diagonal orientation (polars $\parallel [110]/[1\bar{1}0]$) the traces of the domain walls become visible inside the grains, the (110) and $(1\bar{1}0)$ walls intersecting at general angles for general cuts and at right angles if the pseudo-tetragonal c-axis is perpendicular to the cut (Plate I/1 b, c). These two types of wall are expected by theory [11]. The traces of the walls appear rather blurred, leading us to suppose the existence of a much finer subdivision into lamellae not resolved by the microscope. Some crystallites (Plate I/1 b, c) show wall-free darker kernels, apparently indicating a non-transformed tetragonal state.

Sample B (Plate I/2) has been cooled rapidly in air (see 2.1), so that the orthorhombic phase had no time to form. No domains can be seen in the grains and extinction is parallel to the crystallite edges as expected for tetragonal symmetry. Crystallites with the c-axis perpendicular to the surface stay dark upon rotation of the stage (optical axis direction!).

3.2. Single crystals

3.2.1. General remarks.
For the polarization optical domain study the YBCO crystals were either kept attached to the CuO needles as-grown, requiring them to be oriented horizontally by means of a universal stage or spindle stage (Plate I/4 a–e), or they were observed in their flat position after brushing them carefully off the surface.

The monoclinic CuO (Tenorite) crystals are easily recognized between crossed polars by their dark-bluish tint, oblique extinction, well spaced twin lamellae with blue/white contrast upon uncrossing the polars, and often by their needle form. They are easily distinguished from the square or rectangular platelets of YBCO with copper-like tint (Plate II/6 a–b) in the diagonal orientation.

3.2.2. Domain patterns of some crystals.
The crystals 1, 2 and 3 were subjected to X-ray studies. Crystals 1, 2, 3, 5 come from Growth Experiment I, Crystal 4 comes from Experiment II.

Crystal 1 was a square platelet (Fig. 1) with more than ~95% single domain area. In one corner dark parallel lines are seen; they indicate the presence of $(1\bar{1}0)$ domain walls. About 50% of the dark area has the same orientation as the large clear area. Two parallel dark lines, perpendicular to the former ones, represent traces of $(1\bar{1}0)$ walls. Possibly they are further split on a microscopic scale. On Fig. 1 the a- and b-axes,
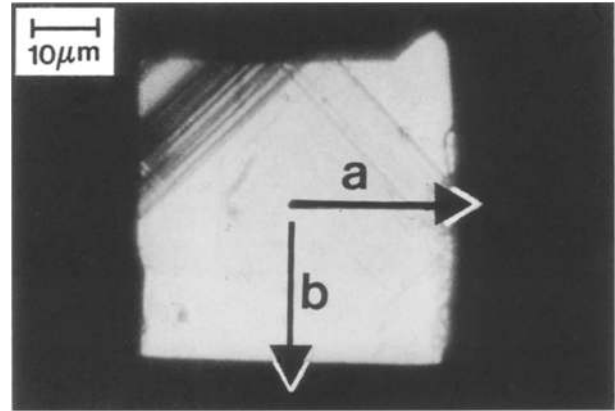
Fig. 1. Crystal 1. A "nearly" single domain crystal of YBCO in diagonal position with compensator in addition position, used for a- and b-axis determination by X-rays→unsplit spots (Fig. 3)
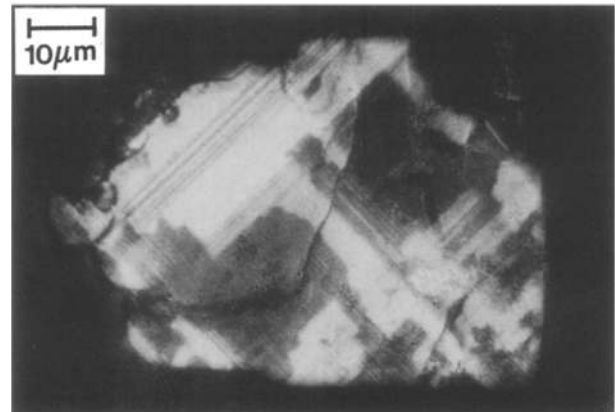
Fig. 2. Crystal 3. Heavily twinned, with "puzzle domain" areas. Contrast with uncrossed polars (see part 7.8). With X-rays→quadrupled spots (Fig. 3)

determined by X-rays, are inscribed. The contrast was obtained with a Berek tilting compensator. Starting from this "master correlation", all the other property relationships, summarised in Table 2 and discussed in part 7, have been established. This crystal was predicted to give non-split reciprocal lattice points on the precession film.

Crystal 2 (Plate II/7 a–c) was composed of a few parallel stripes of unstrained domains, predicted to correspond to the twin pair ①/③ or ②/④ of Fig. 4 and to yield correspondingly a doubling of the reciprocal lattice points, analogous to the reflex doubling found by electron diffraction [20, 21, 29, 30]. In the latter case, the electron beam hit only one of the two possible ensembles of lamellae.

Crystal 3 (Fig. 2) shows a very complicated domain structure which is not fully resolved on the photo-
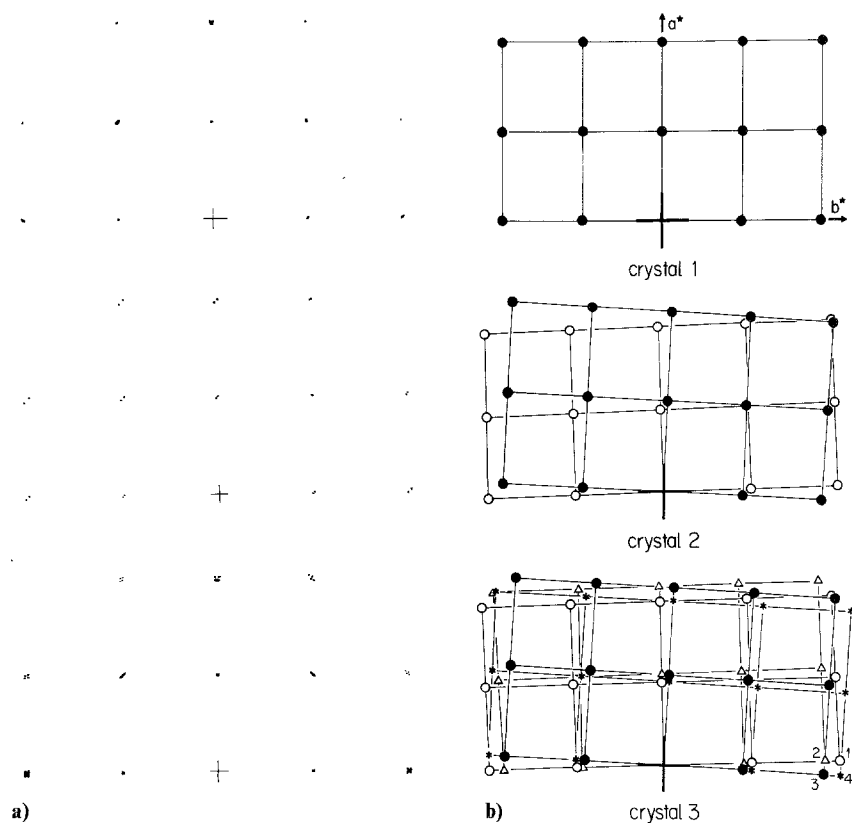
Fig. 3. a Experimental and b calculated reciprocal a^*b^* planes of X-ray precession diagrams for a single domain (crystal 1, Fig. 1), for two domain states (crystal 2, Plate II/7a–c) and four domain states (crystal 3, Fig. 2; idem crystal 4, Plate I/3a–e, Plate II/8a–h)

a)   b)   crystal 3

graph. Beside some larger single domain areas there are also dark ones with very fine lamellae and mutually perpendicular walls in different regions, as schematically shown in Fig. 4. For this sample, a quadrupling of the reciprocal lattice points was expected to be found in agreement with the X-ray results obtained by Sueno et al. [12], but which have not been fully explained.

Crystal 4 (Plate I/3a–e and Plate II/8a–h) is similar to crystal 3, but with much better delimited "puzzle game" like areas of mutually perpendicular fine lamellae, not fully resolved on the photographs. This fine structure can be seen only upon slightly uncrossing the polars (Plate I/3c, e) from the [100]/[010] orientation in which the contrast between the "puzzle" areas nearly vanishes (Plate I/3d), or by means of compensators, e.g. the Laves-Ernst compensator (Plate II/8e, f). With crossed polars along [110]/[1$\bar{1}$0], mutually perpendicular diffuse "traces" of (110) walls are visible (Plate I/3b), whereas the "puzzle" pattern remains entirely hidden for that orientation. (For interpretation see Part 7.8).

Crystal 5 (Plate I/4a–e) represents a frequently found combination between large triangular single domain areas located at the corners of the square platelet,

and a central square composed of "puzzle" areas as found in crystals 3 and 4 (Fig. 2 and Plate I/3a–e) as well as inside the large crystallite of the ceramic sample A (Plate I/1c).

The exact growth conditions and growth mechanisms of the crystals with these different types of domain pattern are not yet understood, but it seems that the large single domain areas have formed under rather stressfree conditions.

4. X-ray studies

Three thin, plate-like crystals were examined by X-ray diffraction at room temperature by using a precession camera (CuK$_\alpha$ radiation). Inspection under the optical microscope revealed that the crystals consisted of nearly one single domain (Crystal 1, Fig. 1), a few domains, separated by (110) walls only (Crystal 2, Plate II/7a–c) and multiple lamellar domains separated by (110) and (1$\bar{1}$0) walls (Crystal 3, Fig. 2). These crystals were oriented such that their faces were perpendicular to the X-ray beam. The resulting photographs contained the reciprocal a^*b^* planes and are represented in Fig. 3a. As expected, the spectrum of the single domain (Crystal 1) consists of unsplit spots forming an orthorhombic reciprocal lattice whereas
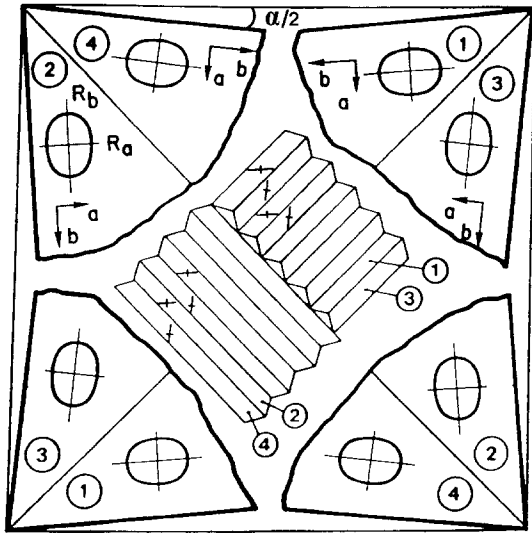
Fig. 4. Schematic representation of the four twin individuals (domain states) of YBCO and their combination into lamellar ensembles. Shear angle α is exaggerated
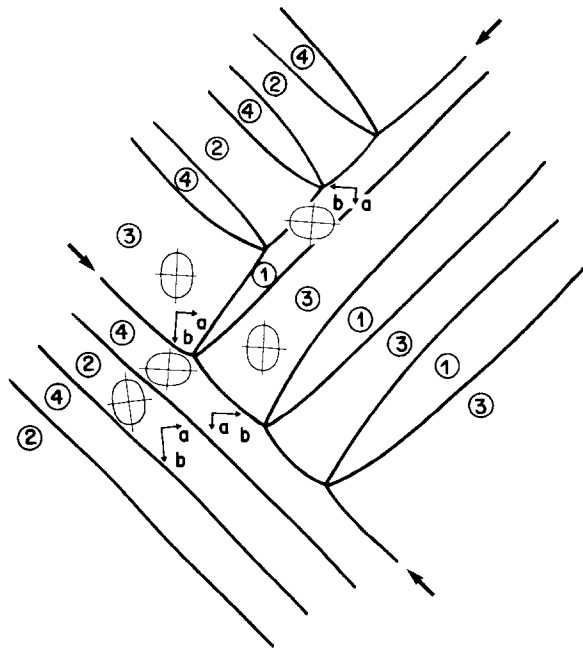

Fig. 5. Schematic interpretation of observed [19] spike domains with the interrupted sequence of mechanically matching by mechanically non-matching domain states at the border line (=frustrated (110) wall, indicated by arrows) between lamellar blocks of "puzzle domain" type

those of the multidomain crystals 2 and 3 consists of split spots which can be interpreted by the superposition of two (Crystal 2) and four (Crystal 3) reciprocal lattices. Their relative orientation (Fig. 3b) corresponds to that expected from the twinning model shown in Fig. 4. The numbering of the four twin indi-

Table 1. Lattice parameters and shear angles α at 298 K for various $Ba_2YCu_3O_{7-\delta}$ crystals

Crystal No.	1 single domain state	2 2 inequivalent domain states	3 4 inequivalent domain states
$a(\text{Å})$	3.820 (3)	3.818 (3)	3.815 (3)
$b(\text{Å})$	3.892 (3)	3.880 (3)	3.885 (3)
$r=a/b$	0.981 (2)	0.984 (2)	0.982 (2)
$\alpha_{obs}(°)$	–	0.87 (4)	1.08 (4)
$\alpha_{calc}(°)$ [a]	–	0.92	1.04

[a] Calculated from the expression: $\alpha_{calc} = 90° - 2 \arctan(a/b)$

viduals in Figs. 3b, 4 and 5 has been chosen in agreement with that adopted by Sueno et al. [12]. The observed shear angles, α, are of the order of one degree, in agreement with the values calculated from the measured lattice parameters (Table 1). It is noteworthy that the strongly twinned Crystal No 3 gives sharp, well separated reciprocal lattice spots. This indicates that the volume percentage of strained, mechanically "unallowed" walls is negligibly small in that sample.

5. Can monoclinic symmetry explain the observed four domain states?

Because the observation of four domain states would point to monoclinic symmetry for a ferroelastic transition from $4/mmm$ according to Aizu [8] and Sapriel [11], let us examine optically whether this is the case for YBCO. There exist three types of domain arrangement corresponding to three possible ensembles of ferroelastic tetragonal→monoclinic point group pairs (called "species" by Aizu [8, 11]), all of which are in principle optically distinguishable:

Case	Monoclinic b-axis	Number of domain states	Number of allowed walls
1	$\parallel [001]_{tetr}$	4	8
2	$\parallel [100]_{tetr}$	4	9
3	$\parallel [110]_{tetr}$	4	9

Case 3 can be easily rejected because extinction in the (001) plane should be along $[110]_{tetr}$ whereas it is observed along $[100]_{tetr}$. Case 2 can also be rejected because twin lamellae separated by (100) walls should be observed. These twins would lead to a puckering of the (001) surface because of the monoclinic shear, usually well observable by specular reflexion in unpolarized light. This is not observed. Furthermore (001) walls are allowed. They could not be found in the

crystallites of the ceramic (sample A), on the polished surface of which (100) and (010)-cuts became to some extent accessible to observation because of the random orientation of the grains. The absence of extended (001) walls is consistent with the electron microscopical observation [24a] that defects with mutually superposed a and b axes (along the c-direction) are of a very localised nature only. Among the 8 allowed walls of case 1 at least two types, i.e. $\|(100)_{tetr}$ and $(1\bar{1}0)_{tetr}$ should occur and one would expect dispersion of the extinction direction in the (001) plane. All this is at variance with the experimental observations.

We can therefore safely conclude that the four observed ferroelastic domains have to be explained by orthorhombic symmetry, in agreement with the numerous published X-ray and neutron data, the great majority of which suggest space group $Pmmm$.

6. Model of the ferroelastic twinning

In Fig. 4 a twinning model is schematically presented that admits orthorhombic symmetry, takes account of the polarization optical observations and the X-ray results (this paper and [12, 31, 32]). By assuming that the lost tetragonal (110) and $(1\bar{1}0)$ mirror planes maintain their orientation relative to the tetragonal metric in the form of orthorhombic twin walls, we end up with four differently oriented domains, at variance with the classical theory [8, 11], predicting that the number of orientation domains n_{01} is equal to the ratio of the order of point group g_0 of the prototype over the order of the point group g_1 of the ferroic phase, i.e. the index $n_{01} = $ order of g_0/order of g_1. This rule holds well for non-ferroelastic transitions, but not for all ferroelastic ones. In a more general approach to orientational twinning, Gratias and Portier [11a] find that the number of domain states can be obtained by the order of the group of the high temperature phase over the order of the point group of the intersection $g_0 \cap g_1$. However, as has been illustrated with examples by Boulesteix [34, 35], in the case of tilting of the structure of the domains – owing to the tendency of the crystal to keep its twin individuals firmly joined along mechanically allowed walls – the point group of the effective intersection and its order (see e.g. [33]) may become lower than that of the domains, thus leading to a higher number of allowed domain states. In the case of YBCO (see model in Fig. 4) this means that the two mirror planes of the mmm-phase containing the c-axis, no longer have the same orientation as in the tetragonal parent phase. As a consequence the effective point group of the intersection is $2/m$ (order 4), leading to the number
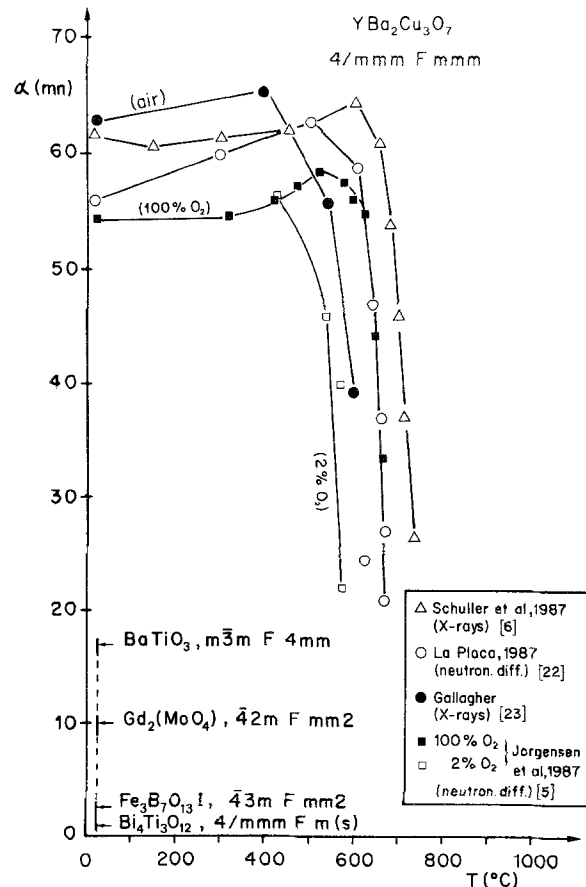
of domains $n_{01} = 16/4 = 4$, in agreement with experiment. It is noteworthy that the above symmetry considerations apply equally well to the problem of epitaxial growth [34, 35].

Recently Shuvalov et al. [13] have also pointed out that the number of possible orientations of ferroelastic domains in real crystals exceeds the number of orientational states determined by the ratio of the orders of the point groups of the prototypic and the ferroic phase. This fact was apparently overlooked in the past for many known ferroelastics because the shear angles $\alpha \equiv 90° - 2 \, \text{arctg}(a/b)$ (see Fig. 6) are often much smaller than in the case of YBCO (about one degree!) and hence the splitting of the reflections in the reciprocal lattice is often not resolved. Under the microscope it is also rather difficult to distinguish between adjacent domains of type ① and ④ or ③ and ② of Fig. 4 if the angle α is only of the order of a few minutes of arc.

Fig. 6. Shear angle $\alpha = 90° - 2 \, \text{arctg}(a/b)$ of YBCO versus temperature, calculated from literature data and compared with α for a few other ferroelastics [24]. Necessary long vertical error bars for YBCO are omitted for clarity. Reference [32] gives a similar temperature dependence of the shear angle

The a- (and b-) axes of the domain pairs ①/③ and ②/④ are mutually tilted by an angle α/2. If such ①/③ or ②/④ twinning is repeated individually in unclamped isolated areas, the ensemble of domains separated (or joined!) by parallel walls remains stress and strain free (Crystal 2, Plate II/7a–c or the individual "puzzle" areas of Plate I/3c, e). However, if ①/③ and ②/④ ensembles meet on (110) walls, an empty space would form (triangular regions in Fig. 4), but which the crystal tends to fill up by increasing the number of lamellae per unit length so that the free elastic energy be minimal. Nonetheless, the border line remains a frustrated region. In practice, the crystal does not leave empty space but it forms wedges (spikes), the points of which are "pulling" the touched walls somewhat off from their ideal [110] direction in the form of cusps, as is often observed in (ferroelectric) ferroelastics. Such spikes and cusps have been observed by electron microscopy on YBCO [19] and we give an interpretation thereof in Fig. 5. One sees that at the border between ensembles with mutually perpendicular walls frustration occurs. For example domain ④ does not find its coherent partner ② and domain ③ does not find its partner ①, etc. Therefore the frustrated boundaries are probably made up of microsteps, alternating with "joints" of dislocations as found for example in mechanical twins of rare earth sesquioxides [34]. The volume percentage occupied by such frustrated walls appears to be quite negligible in the studied crystals (e.g. the irregular boundaries between "puzzle" areas of parallel twins which are made up of small steps of frustrated (110) and (1̄10) walls, Plate I/3c, e) in comparison with the high density of mechanically allowed walls parallel (110) or (1̄10). This is corroborated by the sharp spots of the split reciprocal lattice reflections (Fig. 3a, crystal 3). A high density of frustrated (110) and (1̄10) walls and of the postulated [14] strongly frustrated (001) walls – which have been supposed to be dominating [15] – would be expected to lead to smeared split spots.

In Fig. 6 we have transformed the a, b lattice parameters of YBCO from different authors [5, 6, 22, 23] into the shear angle $\alpha \equiv 90° - 2\arctg(a/b)$ which permits comparison with other ferroelastics [24]. It is noteworthy that shear angles as small as 3 min of arc ($Fe_3B_7O_{13}I$) or 10 min of arc ($Gd_2(MoO_4)_3$) can lead to cracking if mutually perpendicular walls meet. It is thus all the more astonishing that the high shear angle of about 1 degree of YBCO does not lead to autodestruction, except for microcracks which are sometimes observed by electron microscopy [24a] and which would be expected to expand upon temperature cycling. The crystals have, however, different possibilities to escape: i) unhindered growth in a single domain state, ii) formation of domains with only one kind of parallel, allowed (110) walls iii) a high density of allowed (110) and (110)+few frustrated (110) and (1̄10) walls, iv) a potential speciality of YBCO: the possibility of decreasing of shear angle α by means of a redistribution of oxygen on the a- and b-axes under the influence of stress or v) strain relaxation by wall movements which may go on smoothly or discontinuously in analogy with "Barkhausen" jumps.

7. Relationship between orientation of crystallographic axes and that of bireflectance, reflexion and transmission dichroism, contrast generation and form of etch pits of single domains. (All statements of part 7 refer to normal light incidence on (001) facets)

7.1. Determination of orthorhombic a- and b-axis direction

By using a single crystal with about 95% single domain area (Fig. 1) the a- and b-axis directions have been identified by means of an X-ray precession camera. The single domain nature is easily verified by the homogeneous tint obtained if the crystal is viewed in reflected light between crossed polars in the 45°-position and a compensator inserted. Starting from the obtained reference directions obtained by X-rays, the orientation of the following properties has been identified after many cross checks (summary in Table 2):

7.2. Bireflectance

Using the polarizer alone, the bireflectance can be observed in white light (W- or Xe-lamp) or monochromatic light, in the latter case preferably in the red. With the $\vec{E}$-vector of the polarized light oriented along the b-axis, the reflectivity is slightly higher than if oriented along the a-axis. Because the achievable contrast is weak, identification of the a- and b-axes of single domains is easiest where a (110) wall is joining domains with mutually perpendicular a- and b-axes. Then maximum contrast between the domains is obtained if the vibration direction of the polarizer is along [100]. Because of the bireflectance $|R_b - R_a|$ decreasing from the red to the blue [25], contrast between domains vanishes with blue filters.
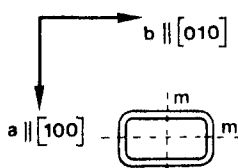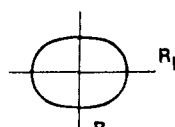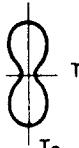
7.3. Reflection dichroism

Because of the anisotropy of reflectivity and the dispersion of bireflectance [25] there is also a slight dif-

ference in tint of the reflected light if the $\vec{E}$-vector of the incident wave is either along a or b (see Table 2). These subtle differences of tint as well as the contrast with monochromatic, e.g. red light are best seen where a domain wall intersects, but they are no longer observable if the crystals have been exposed for some
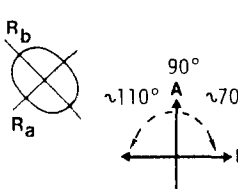
weeks to the humidity of the ordinary atmosphere Plate I/5a, b. However, once the contrast by means of the dichroic tints is no longer observable, the decomposition layer is usually still thin and transparent enough to allow contrast formation with a compensator (see Plate I/5c and Part 7.6).

Table 2. Relationship between orientations of orthorhombic a- and b-axis ($a<b$) with those of bireflectance, reflexion dichroism, transmission dichroism, etch pits, tints generated with analyser rotation and compensators.

Remarks: i) the misorientation between domains ① and ④ or ② and ③ of Fig. 4 is difficult to detect optically and therefore disregarded in this table ii) for the compensators γ means higher refractive index

Orthorhombic axes	$b \| [010]$ $a \| [100]$	identified by means of X-ray precession on single domain orientation of etch pit, symmetry in agreement with the (100) and (010) mirror planes	
Bireflectance	R_b R_a	$R_a(\vec{E}\|\vec{a}) < R_b(\vec{E}\|\vec{b})$ in visible range, particularly in the red	Xe-lamp advantageous, virgin surface necessary
Reflexion dichroism		$\vec{E}\|\vec{a}(R_a)$: dark greenish grey $\vec{E}\|\vec{b}(R_b)$: faint pinkish white $\vec{E}$ at 45° to a and b (mean reflectance): metallic bright	with white light; Xe-lamp advantageous, virgin surface necessary; good contrast in red light; vanishing contrast in blue light
Transmission dichroism	T_b T_a	$\vec{E}\|\vec{a}(T_a)$: yellow bright $\vec{E}\|\vec{b}(T_b)$: dark grey* to black** $\vec{E}$ at 45° to a and b: yellow bright $T_a > T_b$ in visible range	Thickness $*\lesssim 1\ \mu m$; $**\gtrsim 1\ \mu m$

Uncrossing of crossed polars by means of analyser rotation

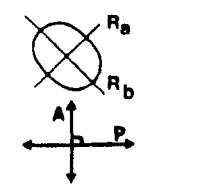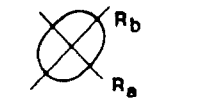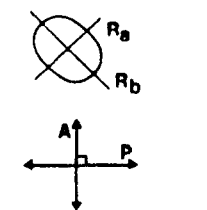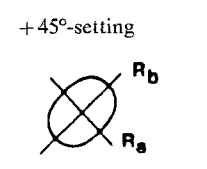|			
a) reflexion mode	R_b R_a 90° ∿110° A ∿70° P	~80°–70° ~100 °C–110°	grey-blue yellow pinkish-straw yellow pinkish-straw yellow grey-blue	White light (*W*-lamp)
b) transmission mode 45°-position	R_b R_a	i) "thick crystals ($\gtrsim 1\ \mu m$) at limit of transmission behave like linear polarizers: extinction at analyser rotation of 45° ii) "thin" crystals ($\lesssim 1\ \mu m$) transmit elliptic light; maximum darkening at analyser rotation $<45°$	See Fig. 7a, b, d and [25] See Fig. 7a, c and [25]
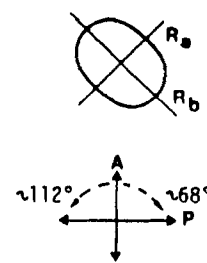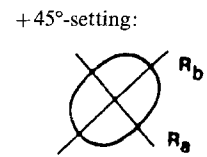
Table 2 (continued)

Compensator effects

Remark: the colours in reflected polarized light depend on reflectivity, bireflectance and their dispersion and have not to be confused with the sequence of Newton colours appearing in transmission (in spite of frequent similarities)

de Sénarmont $\lambda/4$ plate (for $\lambda = 546$ nm) in subparallel position	$-45°$-setting:	Rotation angle of analyser A, with polarizer fixed 90° copper-like 90° copper-like ~83° dark brown ~ 97° yellow-white ~77° grey to black ~103° white ~68° blue grey ~112° white (subtraction) (addition)	White light (W-lamp); the indications of colour are very approximate. The tints may become pale in case of thin decomposition layers owing to attack by water Example: Plate 9 a, c
	$+45°$-setting:	90° copper-like 90° copper-like ~83° yellow-white ~ 97° dark brown ~77° white ~103° grey to black ~68° white ~112° blue grey (addition) (subtraction)	
Berek 4-order tilting compensator (Leitz M) 45°-position	$-45°$-setting:	Tints for two arbitrary tilting angles [21°] ~3.3° dark brown (subtraction) ~4.8° blue grey	White light (W-lamp); the Berek is useful for unequivocal identification of the *a* and *b* axes, but less useful for quantitative measurements in reflected light Example: Plate 4 a–c
	$+45°$-setting	~3.3° yellow white (addition) ~4.8° white	
Laves-Ernst Rotatable Red I ($\Gamma = 551$ nm) λ plate in sub-parallel position	$-45°$-setting	clockwise $(+\sigma)$: sky blue (addition) rotation anti-clockwise $(-\sigma)$: canary yellow (subtraction)	White light (W-lamp); excellent contrast owing to operation close to Red I ("Teinte sensible") Examples: Plates 7 a–c and 8 a–f
	$+45°$-setting	clockwise $(+\sigma)$: canary yellow rotation (subtraction) anti-clockwise $(-\sigma)$: sky blue (addition)	

7.4. Transmission dichroism

On very thin crystals (thickness $\lesssim 1$ μm) it has been discovered that YBCO becomes transparent in the visible with a yellow colour. This is only the case in single domain regions whereas in heavily twinned lamellar areas the crystal remains opaque, even in unpolarized light. This may be due to light scattering
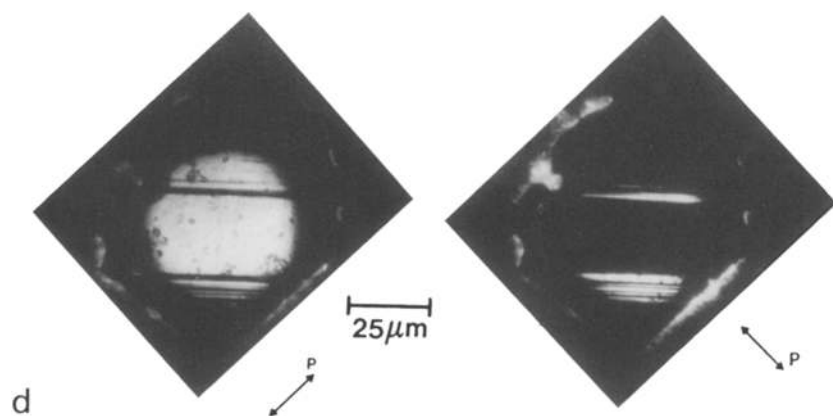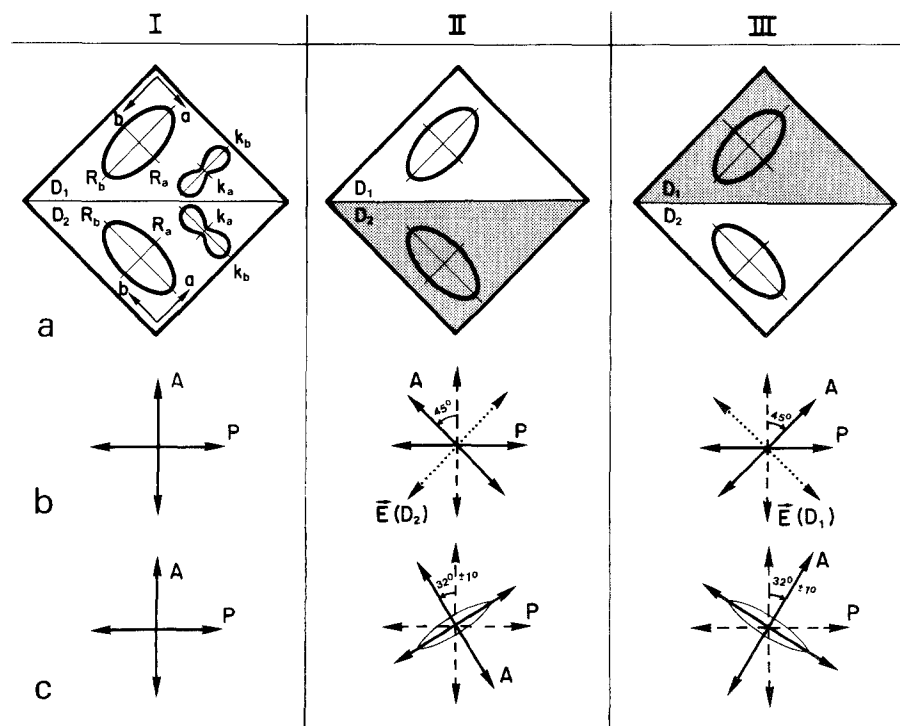
Fig. 7a–d. Transmission dichroism for very thin bi-domains of YBCO, a–c schematic (k_a, k_b absorption coefficients for $\vec{E}\|\vec{a}$, $\vec{E}\|\vec{b}$, resp.) with b linear polarizer behaviour for thickness $\gtrsim 1$ μm, c for thickness $\lesssim 1$ μm, d YBCO platelet of type b viewed with polarizer ($\vec{E}\|\vec{b}$) for both orientations of domain

at the numerous domain walls on which there is no matching of the refractive indices, or to some kind of strongly absorbing defect. On a tiny and very thin bi-domain platelet (extension ~ 40 μm, thickness $\lesssim 0.5$ μm) a strong transmission dichroism has been observed with stronger absorption for $\vec{E}\|\vec{b}$ than for $\vec{E}\|\vec{a}$. Whereas transmission was still observable and the optical density measurable [25] on that crystal for $\vec{E}\|\vec{b}$, slightly thicker crystals (thickness $\gtrsim 1$ μm) behave like linear polarizers (Fig. 7, and Fig. 4 of [25]). Therefore, if the claimed [14] (001) walls really exist, they would lead to strong absorption in unpolarized light because superposed twins with interchanged a- and b-axes can be considered as a set of crossed polarizers!

7.5. Uncrossing of crossed polars by means of analyser rotation

a) Reflexion mode. With perfectly crossed polars there is extinction in the parallel position whereas in the 45°-position ("diagonal"-position) twins with mutually orthogonal a- and b-axes have the same copper-like tint in the as-grown state. More washed-out tints are indicative of a surface layer. In that position apparent traces of (110)/(1$\bar{1}$0)-walls are perceptible and appear dark. Upon uncrossing the polars by rotating the analyser at fixed polarizer (0°)-position, contrast between domains with orthogonal a-, b-axes sets in (see Table 2 and Figs. 8 and 9). For a domain with reflectance R_b along the NW-SE direction the
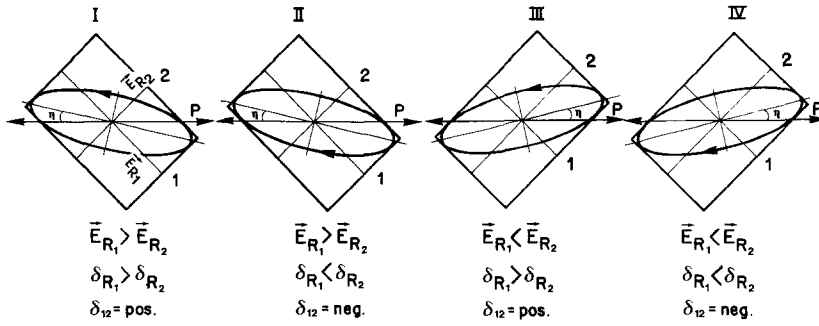
Fig. 8. Four possible states of the elliptical light reflected from an anisotropic absorbing section when linearly polarized light is impinging with $\vec{E}$ in the $E-W$ direction, at 45° to the axes 1,2 of the crystal (diagonal orientation); adapted from Seeliger and Weber [26] for the now standardized (since 1972) $E-W$ orientation of the polarizer of polarizing microscopes. Notation from [26, 27]: $\vec{E}_{R_1}, \vec{E}_{R_2}$ components of electric field vector of reflected wave; $\delta_{R_1}, \delta_{R_2}$ phase difference of partial waves; δ_{12} relative phase shift between partial waves
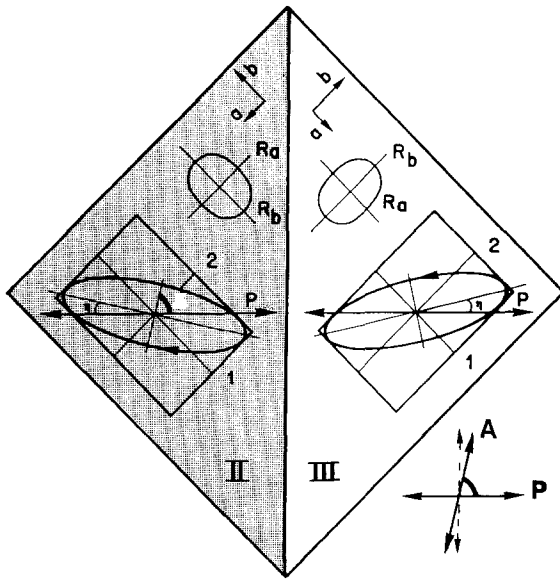
Fig. 9. Relative orientation and sense of rotation of elliptically polarized light reflected from an YBCO bi-domain in the diagonal position and contrast formation upon uncrossing of analyser. Cases II and III of Fig. 8 have been identified for YBCO

copper tint turns via grey-blue to yellow if the analyser azimut goes from 90° to about 80° or 70° and it turns to pinkish and straw yellow for the same analyser position for the domain with R_b along NE-SW.

This contrast formation can be explained by the dispersion of the bireflectance, $\Delta R(\lambda)$. For quantitative data see [25]. It is known [26] that linearly polarized light – impinging with the $\vec{E}$-vector along W-E on a bireflecting, absorbing crystal in the diagonal position – becomes slightly elliptical upon reflexion with the long axis of the ellipse always rotated by an angle

$$\eta = (1/2)\,\text{arctg}\,[(R_1 - R_2)/2(R_1\,R_2)^{\frac{1}{2}}\cos\delta_{12}] \qquad (1)$$

in the direction of the axis of higher reflectivity, i.e. towards R_b in our case. In (1) R_1, R_2 are the principal

reflectivities, R_b and R_a in our case, and δ_{12} is the phase difference between the components of the waves along axes 1 and 2 i.e. b and a. Since $\cos\delta_{12}$ is always close to unity [26], η essentially depends on the bireflectance ΔR and the principal reflectivities. For the diagonal orientation the angle η can also be obtained with sufficient accuracy by the expression [28]

$$\eta \simeq \omega = \text{arctg}\,(\sqrt{R_2}/\sqrt{R_1} - \pi/8) \qquad (2)$$

which does not take account of the relative phase shift δ_{12}.

Thus the dispersion of R causes the dispersion of η, which we can finally use for contrast formation (see Table 2), e.g. if no compensator is at hand.

In order to obtain an idea of the orders of magnitude involved, we mention that $\eta \simeq 3.0$ degrees for the reflectivities measured at room temperature and at $\lambda = 643$ nm [25]. The ellipticity, measured with a Sénarmont compensator is of the order 10^{-2}. More quantitative data will be reported elsewhere.

b) Transmission mode. Between crossed polars – when the domains are in the diagonal orientation – the transmission dichroism is not visible (Fig. 7, case I), but by uncrossing the polars by means of an analyser rotation of 45°, extinction sets in when the vibration direction of the analyser becomes perpendicular to the a-axis, (Fig. 7b, d, cases II, III). For the very thin crystal mentioned above an analyser rotation of much less than 45° led to the darkest position, indicating that elliptical light had emerged from the crystal (Fig. 7c/II, III). The best contrast by means of the dichroism is of course obtained by using a polarizer alone (Fig. 7d).

7.6. Compensator effects

In Table 2 are given the tints for contrast formation that can be achieved by applying the de Sénarmont, the Berek (4-order tilting) and the Laves-Ernst [26, 27] compensators on a hypothetic bi-domain crystal.

In either case we make use of the small ellipticity of the nearly linearly polarized light reflected from the crystal in its diagonal position. Except for the small rotation angle η, the situation comes close to that in transmitted light for a path difference $\Gamma \ll \lambda/4$. For the two domains the rotation sense of the elliptical light and that of the angle η are of opposite sign, thus permitting to create addition and subtraction effects in domains with mutually perpendicular a- and b-axes (Figs. 8, 9).

Advantages and disadvantages of the three compensators for work with YBCO: The Berek compensator allows a rapid and reliable identification of the a/b directions, if the correlation given in Table 2 is consulted. Since the γ-direction (slow ray) is engraved on the compensator and both clockwise and anticlockwise rotation of the compensator give an increase of path difference, practically no error is possible. – For photographic work the Berek is less useful because gradients of hues are produced over the field of view (Plate I/4 b, c), and it is not sufficiently precise for measurements of very small phase shifts.

The determination of the a/b directions with the de Sénarmont and Laves-Ernst compensator requires somewhat more care, because the rotation sense of the measuring screws must not be confused; Table 2 will help.

Both the de Sénarmont (Plate II/6 c and 9 a, c) and Ernst-Laves (Plate II/7 a, c) give homogeneous compensation. The latter compensator is very sensitive and gives bright and vivid colours because it is operating close to Red I. ("teinte sensible").

7.7. Etch pits

During an attempt to thin down a single crystal platelet of YBCO (for optical observation) by means of attack by acetic acid (25%, 3 min) rectangular etch pits were formed (Plate II/6 a–b), consistent with orthorhombic symmetry and with the long side of the rectangle invariably oriented along the b-axes (Table 2). This property may be used for identification of orientation and of defects, but extended homogeneous thinning of the crystal was unsuccessful because of much faster speed of dissolution in the a, b-plane than perpendicular to it. Sometimes, transparency with observable dichroism was achieved in the centre of the etch pits.

7.8. Interpretation of the contrast formation in "puzzle game" domains

It has to be emphasized that the correlations of properties and contrast formation described in 7.1–7.6 and
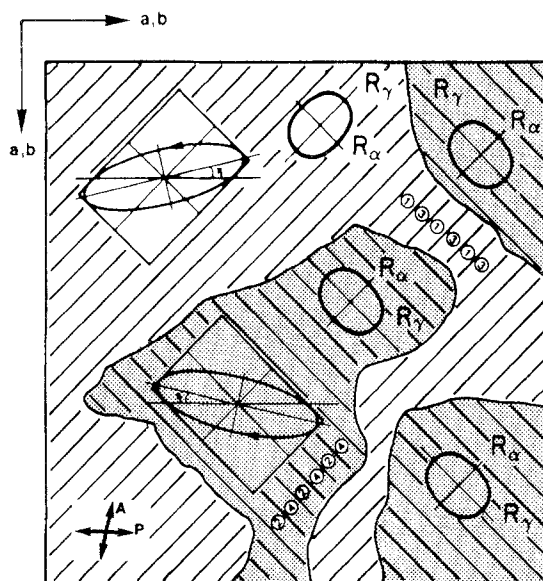
Fig. 10. Schematic representation of the orientation of reflectivity anisotropy in the interior of "puzzle" areas (=pseudo-domains). The numbering of the true domains corresponds to Fig. 4. The contrast formation is based on the state of polarization of the reflected light (inscribed in the lamellar areas) for linearly polarized light impinging with $E\|$east–west; rotation angle η and ellipticity are strongly exaggerated (compare reference [25])

in Table 2 refer strictly only to domains well resolved by the microscope (objective 32 ×, 10 ×), e.g. the large homogeneous triangular domains of Plate I/4 a–e or the domains of Plate II/7 a–c. In areas with "puzzle game" domains, however, an optically anisotropic pseudo-symmetry with pseudo-mirror planes parallel and perpendicular to the tetragonal (110) and (1$\bar{1}$0) planes is observed (Fig. 10): there is strong extinction with diffuse dark lines along [110]/[1$\bar{1}$0] with the crossed polars parallel [110]/[1$\bar{1}$0] (=diagonal position for the large domains) (Plate I/3 b) and a weak but well perceptible brightening with the crossed polars parallel [100] (Plate I/3 d), corresponding to the diagonal position of the pseudo-symmetry which is the extinction position for the large domains. Starting from the latter orientation, excellent contrast is obtained between mutually perpendicular areas of parallel stripes, either by uncrossing of the polars (Plate I/ 3 c, e, 4 d, 4 e) or by means of compensators (Plate II/ 8 e–h), based on the same principle as explained in Fig. 9, but with the difference that the principal axes of bireflectance are oriented at 45° to the true orthorhombic axes [25]. The contrast between the lamellae inside a "puzzle" domain is extremely weak. It is probably caused by regions with different distances between walls and a weight ratio between domain states (e.g. ② and ④) differing from unity. For equi-

distant walls and a weight ratio of unity the lamellae would be expected to become entirely invisible. Indeed in some crystals the density and regularity of the (110) walls was so high that the "puzzle" domains mimicked homogeneous single domain areas. By means of the established sense of analyser rotation (Plate I/3 c, e and Fig. 10) it is, however, possible to deduce the hidden orientation of the walls in such regions. The pseudo-symmetry is also manifested by a weak reflexion dichroism visible in white light with the vibration direction of a polarizer parallel [110] or [1$\bar{1}$0] alone. The areas for which the polarizer is perpendicular to the stripes, appear greenish blue (Plate I/3 a). It has been shown elsewhere [25] that the bireflectance inside the "puzzle domains" is characterized by a higher reflectivity, i.e. a higher optical conductivity for light impinging with the $\vec{E}$-vector parallel to the walls than for $\vec{E}$ perpendicular to the walls. This means that the reflectivity "sees" the scattering (resistivity) of the walls.

8. On the origin of bireflectance and associated contrast formation between domains

Measurements of the anisotropic a, b-plane reflectivity of YBCO single domains versus wavelength in the visible have shown [25] an increase of bireflectance from the blue to the red which is generated by the rise of reflectivity for light polarized $\vec{E}\|\vec{b}$ only, whereas, for $\vec{E}\|\vec{a}$ essentially wavelength independent reflectivity is found in the visible. The increase of reflectivity for $\vec{E}\|\vec{b}$ is caused by the tail of the plasma edge (the edge is found at about 1.5 eV for polydomain crystals [36]) "peeping" into the visible for $\vec{E}\|\vec{b}$ only, whereas for $\vec{E}\|\vec{a}$ the reflectivity is essentially determined by the optical background dielectric constant due to the bound electrons. This means that the effective optical mass m^* of the free electrons must be larger for $\vec{E}\|\vec{a}$ than for $\vec{E}\|\vec{b}$, thus pushing the plasma edge for $\vec{E}\|\vec{a}$ to smaller energies outside the visible range.

Reflectivity measurements on a, c- and b, c-plane domains have not yet been performed, but observation of (100)-cut crystallites on polished ceramic sections with crossed polars in the diagonal position show a pattern of clear and dark stripes parallel [001] (Fig. 11 b), made up of two kinds of individual, one showing strong bireflectance with extinction parallel [100]/[001] and clearing up in the diagonal orientation, the other one staying dark between crossed polarizers for any orientation of the microscope stage. This behaviour can be explained. As was shown by Tozer et al. [37], the normal state electric conductivi-

a

b
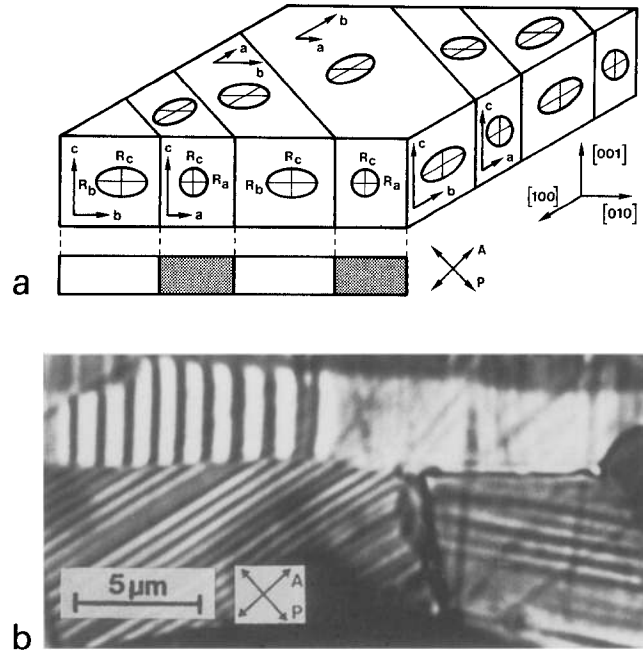
Fig. 11 a and b. Representation of orientation of reflectivity anisotropy on pseudotetragonal (001), (100) and (010) facets, a schematic, with schematic contrast on (100) facet with crossed polars in diagonal position; note that the representation surface of reflectivity is of higher rank than the ellipsoid [28, p. 86]. **b** top left hand corner: a, c/b, c stripe domains on crystallite of ceramic (sample A) with (100) plane approximately horizontal a, c domains dark, b, c domains clear; objective 100 × /oil, ocular 10 ×

ty parallel to the c-axis is semiconductor-like. This will cause the optical effective mass m^* for $\vec{E}\|\vec{c}$ to be higher than that for $\vec{E}\|\vec{b}$, thus pushing the plasma edge and its tail for $\vec{E}\|\vec{c}$ to lower energies outside the visible range, as is the case for $\vec{E}\|\vec{a}$ [25], in agreement with band calculations [38]. As a consequence the reflectivity of an a, c-cut will be nearly isotropic, because only the relatively small differences of the real part of the refractive index (i.e. birefringence) will lead to some very small anisotropy of reflectivity ($R_c \approx R_a$). We can therefore identify the a, c plane domains as those staying dark all the time when viewed with crossed polars and rotating the microscope stage, whereas the b, c plane domains must be those showing strong bireflectance with the reflectivity (R_b) for $\vec{E}\|\vec{b}$ higher than that (R_c) for $\vec{E}\|\vec{c}$ (Fig. 11 a, b).

It is noteworthy that the a, c and b, c-plane domains are also well distinguishable with a polarizer alone oriented $\vec{E}\|\vec{a}$, $\vec{b}$, the b, c-domains appearing very bright and the a, c-domains dark ($R_b > R_a$). After rotation of the polarizer by 90° the contrast vanishes since in both domains the $\vec{E}$-vector oscillates along the c-axis.

9. Conclusions

i) Polarized light microscopy is found to be a powerful tool to evaluate the ferroelastic domain structure of YBCO, complementing advantageously the more penetrating techniques like electron microscopy and X-ray analysis to gain a view of the anisotropic bulk properties.

ii) On the basis of the X-ray and optical results the observed presence of four (instead of two) ferroelastic domains is found compatible with orthorhombic symmetry, at variance with former group theoretical predictions, but consistent with symmetry considerations by Gratias and Portier [11a], Boulesteix [34, 35] and Shuvalov et al. [13] on analogous ferroelastic twinning.

iii) In single crystals the volume occupied by the ferroelastically allowed, i.e. strain free (110) and ($1\bar{1}0$) walls exceeds by far that of the frustrated (110) and ($1\bar{1}0$) walls. In an annealed, coarse grained ceramic the situation was found to be similar.

iv) On very thin single domains (thickness about 1 μm) YBCO was found to be transparent in the visible, with a strong dichroism, leading at the limit of transparency to a linear polarizer behaviour. The transmission dichroism and strong absorption are consistent with $O^{2-} \rightarrow Cu^{3+}$ charge transfer [25].

v) Different techniques – with and without compensators – for the generation of contrast between ferroelastic domains, all based on bireflectance, reflexion dichroism and transmission dichroism, have been evaluated and correlated with the crystallographic axes. On that basis a rapid judgment of the domain state of single crystals and ceramics is now possible. More quantitative data will be published elsewhere [25].

vi) Lamellar ensembles of ferroelastic domains with parallel (110) or ($1\bar{1}0$) walls generate strong bireflectance with principal axes rotated by 45° relative to the true orthorhombic metric if the distance between walls is beyond the resolution of the optical microscope. The orientation of bireflectance of the lamellar ensembles, i.e. the reflectivity for $\vec{E}$ parallel to the walls higher than perpendicular to them, is a direct evidence for the scattering (resistance) of the walls. This may be taken as a warning because physical tensorial properties other than the optical representation surfaces, such as DC- and AC-conductivity, thermal conductivity, susceptibility etc. can be expected to respond in an analogous way. Depending on the mutual weight and orientation of large single domains and lamellar ensembles, very different "non-reproducible" experimental results may therefore be obtained in physical measurements on polydomain single crystals without preceding optical characterization.

vii) The good optical contrast achievable in reflected polarized light between ferroelastic domains can be attributed to the free electron contribution to reflectivity from the tail of the plasma edge for the polarization $\vec{E} \| \vec{b}$ only.

References

1. Syono, Y., Kikuchi, M., Oh-ishi, K., Hiraga, K., Arai, H., Matsui, Y., Kobayashi, N., Sasaoka, T., Muto, Y.: Jpn. J. Appl. Phys. **26**, L498 (1987)
2. Eaglesham, D.J., Humphreys, C.J., McN.Alford, N., Clegg, W.J., Harmer, M.A., Birchall, J.D.: Appl. Phys. Lett. **51**, 457 (1987)
3. Iijima, S., Ichihashi, T., Kubo, Y., Tabuchi, J.: Jpn. J. Appl. Phys. **26**, L1478 (1987)
4. Brokman, A.: Solid State Commun. **64**, 257 (1987)
5. Jorgensen, J.D., Beno, M.A., Hinks, D.G., Soderholm, L., Volin, K.J., Hitterman, R.L., Grace, J.D., Schuller, I.K., Segre, C.V., Zhang, K., Kleefisch, M.S.: Phys. Rev. B**36**, 5731 (1987)
6. Schuller, I.K., Hinks, D.G., Beno, M.A., Capone II, D.W., Soderholm, L., Locquet, J.-P., Bruynseraede, Y., Segre, C.U., Zhang, K.: Solid State Commun. **63**, 385 (1987)
7. Wondratschek, H., Jeitschko, W.: Acta Crystallogr. A**32**, 664 (1976)
8. Aizu, K.: Phys. Rev. B**2**, 754 (1970)
9. Fousek, J., Janovec, V.: J. Appl. Phys. **40**, 136 (1969)
10. Fousek, J.: Czech. J. Phys. B**21**, 955 (1971)
11. Sapriel, J.: Phys. Rev. B**12**, 5128 (1975)
11a. Gratias, D., Portier, R.: Proceedings of the 3rd International Conference on Martensitic Transformations, Cambridge USA, 24–29 June 1979, pp. 177–182
12. Sueno, S., Nakai, I., Okamura, F.P., Ono, A.: Jpn. J. Appl. Phys. **26**, L842 (1987)
13. Shuvalov, L.A., Dudnik, E.F., Wagin, S.V.: Ferroelectrics **65**, 143 (1985)
14. Raveau, B., Michel, C.: European Workshop on: High T_c Superconductors and Potential Applications, Genova, 1–3 July 1987, programme pp. 45–56
14a. Hervieu, M., Domengès, B., Michel, C., Provost, J., Raveau, B.: J. Solid State Chem. **71**, 263 (1987)
15. Deutscher, G., Müller, K.A.: Phys. Rev. Lett. **59**, 1745 (1987)
16. Damento, M.Y., Gschneider, K.A. Jr., McCallum, R.W.: Phys. Lett. **51**, 690 (1987)
17. Dinger, T.R., Worthington, T.K., Gallagher, W.J., Sandstrom, R.L.: Phys. Rev. Lett. **51**, 690 (1987)
18. Dinger, T.R., Cook, R.F., Clarke, D.R.: Appl. Phys. Lett. **51**, 454 (1987)
19. Takei, H., Takeya, H., Iye, Y., Tamegai, T., Sakai, F.: Jpn. J. Appl. Phys. **26**, L1425 (1987)
20. Tanaka, M., Terauchi, M., Tsuda, K., Ono, A.: Jpn. J. Appl. Phys. **26**, L1237 (1987)
21. Iijima, S., Ichinashi, T., Kubo, Y., Tabuchi, J.: Jpn. J. Appl. Phys. **26**, L1478 (1987)
22. La Placa, in Malozemoff, A.P., Grand, P.M.: Z. Phys. B – Condensed Matter **67**, 275 (1987)

322

23. Gallagher, W.J., Sandstrom, R.L., Dinger, T.R., Shaw, T.M., Chance, D.A.: Solid State Commun. **63**, 147 (1987)
24. Schmid, H., Schwarzmüller, J.: Ferroelectrics **10**, 283 (1976)
24a. Raveau, B.: Private communication
25. Schmid, H., Rivera, J.-P., Clin, M., Williams, A., Burkhardt, E.: International Conference HTSC-ME²S, February 29–March 4, 1988, Interlaken, Switzerland; Physica C**153–155**, 1748 (1988)
26. Seeliger, E., Weber, K.: Fortschr. Mineral. **45**, 147 (1968)
27. Rabe, H.: Fortschr. Mineral. **61**, 243 (1983)
28. Galopin, R., Henry, N.F.M.: Microscopic study of opaque minerals, p. 95. Cambrigde: Heffer 1972
29. Alario-Franco, M.A., Chaillout, C., Capponi, J.J., Chenevas, J.: Mater. Res. Bull: **22**, 1685 (1987)
30. Chaillout, C., Alario-Franco, M.A., Capponi, J.J., Chevenas, J., Hodeau, J.L., Marezio, M.: Phys. Rev. B: **36**, 7118 (1987)
31. Strobel, P., Capponi, J.J., Chaillout, C., Marezio, M., Tholence, J.L.: Nature **327**, 306 (1987)
32. Hodeau, J.L., Chaillout, C., Capponi, J.J., Marezio, M.: Solid State Commun. **64**, 1349 (1987)
33. Hahn, T. (ed.): International tables for crystallography, Vol. A: Space group symmetry, p. 775. Dordrecht, Boston: Reidel 1983
34. Boulesteix, C. In: Handbook on the physics and chemistry of rare earths, Chapt. 44, pp. 321–386. Amsterdam: North Holland 1982
35. Boulesteix, C.: Phys. Status Solidi (a) **86**, 11 (1984)
36. Schlesinger, Z., Collins, R.T., Kaiser, D.L., Holtzberg, F.: Phys. Rev. Lett. **59**, 1958 (1987)
37. Tozer, S.W., Kleinsasser, S.W., Penney, T., Kaiser, D., Holtzberg, F.: Phys. Rev. Lett. **59**, 1768 (1987)
38. Yu, J., Massida, S., Freemann, A.J., Koeling, D.D.: Phys. Lett. A **122**, 203 (1987)

H. Schmid, E. Burkhardt, W. Brixel, M. Clin, J.-P. Rivera
Université de Genève,
Département de Chimie Minérale, Analytique et Appliquée
30, quai Ernest Ansermet
CH-1211 Genève 4
Switzerland

E. Walker, J.-L. Jorda
Université de Genève
Département de Physique de la Matière Condensée
24, quai Ernest Ansermet
CH-1211 Genève 4
Switzerland

M. François, K. Yvon
Université de Genève
Laboratoire de Cristallographie aux Rayons-X
24, quai Ernest-Ansermet
CH-1211 Genève 4
Switzerland